ORIGINAL ARTICLE

Assessment of vegetation dynamics in Upper East Region of Ghana based on wavelet multi-resolution analysis

J. A. Quaye-Ballard[1] · T. M. Okrah[1] · S. A. Andam-Akorful[1] · A. Awotwi[2] · W. Osei-Wusu[1] · T. Antwi[1] · X. Tang[3]

Abstract

Vegetation variation offers significant information for environmental planning, management, sustainability and prompts caution of ecosystem degradation, particularly for the semiarid regions. Normalized difference vegetation index (NDVI) discloses the coverage growth situation, biomass and photosynthesis strength of vegetation and land-cover alterations. Wavelet was used to decompose NDVI time series into subseries at various timescales. This study used a multi-resolution analysis in association with Mann–Kendall and Sen's Slope at 95% confidence interval to determine the trends in vegetation dynamics at the Upper East Region (UER) of Ghana. GIMMS NDVI3g time series was used to evaluate the performance of the vegetation at seasonal, interannual and intraannual timescale from 1982 to 2015. The results showed that the variability in NDVI in the region is annually significant. At the seasonal level, the whole surface area showed negative vegetation trend. In terms of the intraannual changes, 11.76% of the surface area showed critical patterns. At the interannual scale, results revealed that 4.40% of the surface area demonstrated significant patterns, while 95.60% indicated nonsignificant pattern. Overall, there was negative performance in the vegetation growth from 1982 to 2015. The 16.6% decrease in vegetation dynamics can be attributed to anthropogenic activities. The results from this study would benefit and provide helpful assistance to water resources managers, agricultural and ecological development officers for sustainable planning of UER.

Keywords Wavelet transform · Multi-resolution analysis · GIMMS NDVI3g · Vegetation dynamics · Trend analysis

Introduction

The vegetation in Upper East Region (UER) is continually changing due to climate-imposed stresses and human-induced factors at spatial and temporal scales (USAID 2011). Vegetation can be partitioned into natural, seminatural and cultivated. The natural vegetation is the virgin forest not hindered by human activities. Seminatural vegetation is when vegetation is influenced by human activities but has recovered to a degree that species constituents and ecosystem processes are in a course of attaining their undisturbed status. Cultivated vegetation are those areas which are artificially planted and maintained, e.g., hayfields and pastures (Sprugel 1991). The vegetation in UER consists of natural, seminatural and cultivated in a form of forest reserves, Government Reforestation Program and cropland, respectively (Yiran et al., 2012). These vegetation types are important for raising livestock and other livestock products such as milk for human consumption in UER (USAID 2011). Globally, the vegetation compositions are changing at spatial and temporal scales and these can be attributed to natural and artificial reasons. The changes in vegetation can be classified into vegetation phenology, which are driven by photosynthetic and land-cover change which involves permanently replacing vegetation at a particular location (Martínez and Gilabert 2009; Ibrahim et al. 2015). The vegetation dynamics in West Africa have been firmly linked to both climatic variability and anthropogenic activities (Knauer et al. 2014). Monitoring to identify changes in vegetation over some time provides information for detecting the causes and rates of change in ecosystems (Omuto et al. 2010).

✉ A. Awotwi
   awor73@yahoo.com

[1] Department of Geomatic Engineering, Kwame Nkrumah University of Science and Technology (KNUST), Kumasi, Ghana

[2] Department of Earth and Environmental Sciences, University for Development Studies (UDS), Navrongo, Ghana

[3] Department of Civil Engineering, University of Nottingham Ningbo China, Ningbo, China

Researching into climate- and human-induced changes on vegetation and their relationships is vital in managing the ecosystem (Mberego et al. 2013). Normalized difference vegetation index (NDVI) is one technique for detecting and monitoring the spatiotemporal trends of vegetation to detect land-cover and land-use change (Bruce and Byrd, 2006; Galford et al. 2008; Omuto et al. 2010; Campos and Marcelo 2012; Liu and Menzel 2016). The temporal dynamics of NDVI values at a location is a basic information for studying observed phenomena in vegetation (Epinatl et al. 2001). Additionally, NDVI values can be utilized as a measure of aboveground land-cover changes, e.g., land degradation, fires, flooding and farming (Campos and Marcelo 2012). The ability of any framework to detect change depends on its capacity to account for variability at one scale (e.g., seasonal variations) while identifying change at another (e.g., multi-year trends) (Martínez and Gilabert 2009). As a result, changes in the ecosystems conditions can be grouped into three classes: seasonal change which is driven by annual temperature and rainfall interactions affecting plant phenology or proportional land-cover types with different plant phenology; slow change such as interannual climate variability (e.g., patterns in mean annual rainfall) or slow change in managed/degraded land; and sudden change, caused by disturbances such as deforestation, urbanization, floods and fires (Geerken and Ilaiwi 2004; Martínez and Gilabert 2009; Jia et al. 2014; Awotwi et al. 2015; Liu and Menzel 2016; Rimkus et al. 2017; Awotwi et al. 2019).

In order to determine the essential elements influencing the reduction in vegetation cover to support policies and sustainable management, researchers are adopting new methods and systems for an in-depth understanding about changes in vegetation cover elements (Roder and Hill 2009). Various studies have been utilizing relationships between NDVI and climatic variables such as rainfall and temperature to show degradable territories or productivity in vegetation (Ichii et al. 2002; Al-Bakri and Taylor 2003; Nischitha et al. 2014). Notwithstanding, these investigations hardly reveal the increasing or decreasing patterns and fail to determine the behavior of periodicity in climatic variable time series. Different studies used principal component analysis (PCA) to show the spatial variability in NDVI time series (Mberego et al. 2013). In recent times, numerous researchers are embracing wavelet transform (WT), which can decompose and determine localization or power concentration in NDVI time series (Lunetta et al. 2006; Galford et al. 2008; Campos and Marcelo 2012). Some researchers combined WT with Mann–Kendall trend test and Sen's Slope to evaluate patterns in climatic variables (e.g., Martínez and Gilabert 2009; Joshi et al. 2016; Liu and Menzel 2016). For example, Martínez and Gilabert (2009) and Liu and Menzel (2016) combined WT, Mann–Kendall trend test and Sen's Slope estimator to determine critical long- and short-term pattern in NDVI time patterns.

The objective of this is to assess intraannual, interannual and human activities affecting vegetation in UER. This will help to assess the vegetation changes in an agriculture region of Ghana due to frequent drought episodes and overuse of natural resource from increased population (USAID 2011; Yiran et al. 2012; Ayumah 2016). For example, Ayumah (2016) demonstrated low harvest yield at the northeastern part of UER because of continuous dryness. Yiran et al. (2012) uncovered dynamic vegetation degradation at the same region as a result of climatic stress factors such as drought- and human-induced activities such as overgrazing, deforestation, bush burning, etc. In this study, multi-resolution analysis (MRA) was used in breaking down NDVI time series in order to analyze intraannual, interannual trend and human-induced activities in UER. The Mann–Kendall trend test and Sen's Slope estimator were also used to show the areas of significant trend. A computer algorithm has been developed for the implementation of the MRA and determining the significant trend analysis at 95% confidence interval.

Materials and methods

Study area

The UER is located in the northeastern part of Ghana between latitude 10° 20′ N and 11° 12′ N and longitude 0° 03′ E and 1° 25′ W (Fig. 1). It has a total land surface of around 8842 km^2, representing 2.7% of land area of Ghana (Ghana Statistical Service 2014). The climate of the UER is dry submoist with average temperature of 38 °C. The region experiences a unimodal rainfall pattern, which begins in April/May (46.7/92.0 mm) and crests in August (255.0 mm) before it stops in October (53.2 mm). The topography is dominated by relatively undulating plains and gentle slopes ranging from 1 to 5% gradient with some few rock outcrops and some highland slopes (Ghana Statistical Service 2014). The vegetation is Sudan Savannah with short grasses and wide-scattered Shrub (Yiran et al. 2012). The region is drained by the Red, White Volta and Sissili Rivers with small dam reservoirs for irrigation farming and domestic use during the dry season (Leemhuis et al. 2009). The region is characterized by low rainfall, high temperatures, land degradation, deforestation and overgrazing (Ministry of Food and Agriculture 2017). The main economic activity of the people is farming, which employs about 80% of the total population. The rest of the population involves in trading and craftsmanship like 'smock' weaving, pottery and basketry (Ghana Statistical Service 2014).
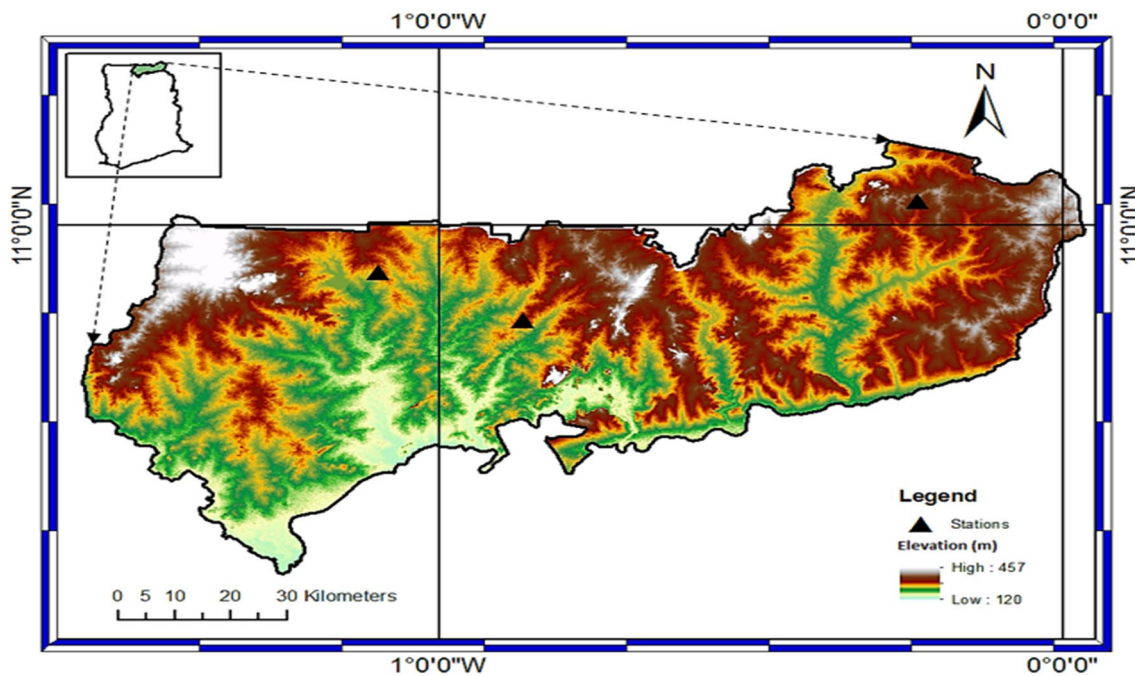
Fig. 1 Study area and location of rain gauge stations

Data description

The NDVI data used in this study are the third-generation version, GIMMS NDVI3g, from Global Inventory Modeling and Mapping Studies. The GIMMS NDVI3g is derived from National Oceanic and Atmospheric Administration (NOAA) satellite carrying Advanced Very High-Resolution Radiometer (AVHRR) sensor (Dahlin et al. 2015; Liu and Menzel 2016). GIMMS NDVI3g dataset is a worldwide vegetation condition data that has a spatial resolution of 0.0833° and a timescale of 15 days (Ibrahim et al. 2015). Since 2011, the GIMMS NDVI dataset has been improved and called NDVI3g. GIMMS NDVI3g ranges from 1981 to 2015. The GIMMS NDVI data are corrected from blunders, for example, residual sensor degradation, constant cloudiness globally, orbital drift, view geometry and solar zenith angle (Sharma 2006; Ibrahim et al. 2015; Liu and Menzel 2016). GIMMS NDVI3g data were chosen due to their long-term continuous satellite-derived NDVI time series.

Wavelet transform

Wavelet transform (WT) has been utilized in different research fields to investigate signal and has shown superiority in analyzing frequency and time localization in a time series (Martínez and Gilabert 2009; Santos and Freire 2012). A wavelet is characterized as a small wave with finite and concentrated energy in time and space (Sharma 2006). This makes wavelet a powerful tool for investigating

nonstationary, time-invariant and periodicity in signals (Santos and Freire 2012; Ramana et al. 2013; Dyn et al. 2016; Sun et al. 2016). Various strategies have been utilized to investigate variety in signals, e.g., harmonic and Fourier transform, but their disadvantage in assuming a stationarity and linearity makes them not ideal for analyzing nonstationary data, e.g., climatic variables (Martínez and Gilabert 2009; Santos and Freire 2012; Baidu et al. 2017). WT decomposes time series or signals into time–frequency space, enabling the determination of localized variation in the time series (Torrence et al. 1998; Santos and Freire 2012; Ramana et al. 2013; Sun et al. 2016). In applying WT, a small wavelet with finite length called 'Mother wavelet' is used to decompose the original time series. Mother wavelet is a mathematical function with zero mean and localized in time and space (Torrence and Compo 1998). As indicated by Torrence and Compo (1998), there are conditions that must be adhered to when choosing a mother wavelet, for example, orthogonality or nonorthogonality, real or complex function, shape and width. There are different types of mother wavelets, e.g., Symmlet, Haar, Daubechies, Gaussian, Molert, etc. The length of a wavelet ranges from positive to negative infinite such that by varying the length of the wavelet, both low- and high-frequency components can be determined (Martínez and Gilabert 2009). Localized variation or power concentration of variance in a signal can be viewed through spikes, discontinuity, etc., in a time series which can easily be detected. This study employs Daubechies (db) and Molert (morl) mother wavelet functions due to their ability to

detect localized pattern in time series and their full scaling and translational orthonormality properties and popularity in climatic studies (Nalley et al. 2012; Joshi et al. 2016; Liu and Menzel 2016). Usually, in a one-dimensional view, a wavelet is formed from the connection between the mother wavelet (ψ) and the scaling capacity (ϕ). For example, consider Mother wavelet consisting of the product of a plane wave with a Gaussian modulation (Santos and Freire 2012) as indicated below:

$$\psi_{a,b}(t) = \frac{1}{\sqrt{a}} \psi\left(\frac{t-b}{a}\right) a > 0, \ -\infty < b < \infty \tag{1}$$

where a is the scale parameter and b determines the location of the wave in time t.

The parameter b can be utilized to choose bit of the signal at any time t. Parameter a is the dilation parameter of the wavelet, which can be varied at a scale. Wavelet must fulfill two primary conditions: (1) integrating ψ to zero and (2) integrating ψ^2 to zero as illustrated below.

$$\int_{-\infty}^{+\infty} \psi(t)\mathrm{d}t = 0 \tag{2}$$

$$\int_{-\infty}^{+\infty} \psi^2(t)\mathrm{d}t = 1 \tag{3}$$

Equation (2) means that the function ψ oscillates around zero, and Eq. (3) makes the function ψ localized in a finite width interval. These conditions act as constraints in creating a small wave or wavelet (Martínez and Gilabert 2009). In practice, a third condition known as admissibility which allows reconstruction of the wavelet from its continuous wavelet transform needs to be met (Torrence and Compo 1998). The three conditions ensure that the energy in the time series is maintained after transform (Torrence and Compo 1998; Martínez and Gilabert 2009; Santos and Freire 2012). The two main types of WT are continuous wavelet transform (CWT) and discrete wavelet transform (DWT). CWT adopts a smooth continuous function to decompose a time series. Consider a signal $f(t)$ and a 'mother wavelet' $\psi_{a,b}$; then, the CWT is given as:

$$W(a,b) = \int_{-\infty}^{+\infty} \bar{\psi}_{a,b}(t)f(t)\mathrm{d}t \tag{4}$$

$$W(a,b) = \frac{1}{\sqrt{a}} \int_{-\infty}^{+\infty} \bar{\psi}_{a,b}\left(\frac{t-b}{a}\right)f(t)\mathrm{d}t. \tag{5}$$

Integrating Eq. (4) results into (5), the outcome $W(a, b)$ for any timescale parameter is the wavelet coefficient at an location specified by a. The integration is repeated for all the combinations of parameters a and b leading to the decomposition in both time and space. The wavelet coefficient would then be able to be interpreted as variation in the signal through time. CWT is smoother and provides a fast way for analyzing small array signals. A detailed literature on CWT can be found in Torrence and Compo (1998). For DWT, a discrete wavelet function is utilized which adjusts well to a given signal. The scaling parameter for DWT is 2 where a is 2^j and j is the level of decomposition. DWT involves filtering and downsampling. The filtering process involves using different cutoff frequencies at different scales (a), and it is applied to analyze both high and low frequencies in a signal. The high filters are known as details (D) component and retain the detail features of the signal, while the low filters are known as approximations (A) component and retain small features in a time series (Sharma 2006; Martínez and Gilabert 2009). The DWT decomposition of signal (S) into details (D) and approximations (A) component is shown in Fig. 2.

In downsampling process, the resolution of the signal is reduced to remove some of the samples in a signal. This enables the detailed component of the signal to be assessed. The wavelet coefficient (W) of a DWT is derived by considering a signal $f(t)$, 'mother wavelet' $\psi_{a,b}$ and a decomposition level j as follows:

$$\psi_{j,k}(t) = 2^{-j/2}\psi(2^{-j}t - k) \tag{6}$$

$$W_{j,k} = 2^{-j/2} \int_{-\infty}^{+\infty} f(t)\bar{\psi}(2^{-j}t - k)\mathrm{d}t \tag{7}$$

where $j = 1, 2, 3,..., N$.

The detail (D) part which is determined by the high filter is identified with wavelet coefficient (W), while the approximation (A) which is the smooth representation of
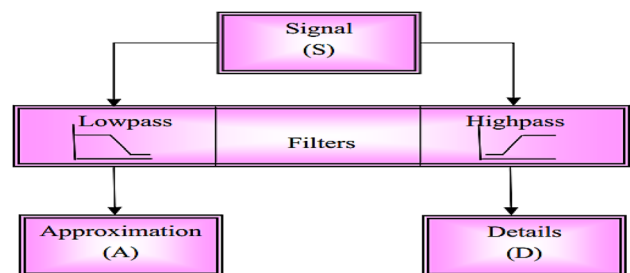

Fig. 2 Discrete wavelet decomposition of signal into detail and approximation (adopted from Sharma (2006)

the signal ($f(t)$) is controlled by the scaling function (Martínez and Gilabert 2009).

Multi-resolution analysis (MRA)

MRA is a hierarchical application of DWT in which a signal is successively decomposed into different levels and filtered utilizing high and low filters (Martínez and Gilabert 2009). The connection between the detail (D) and approximation (A) components is in the proportion of 2:1. The decomposed signal (*S*) is then reconstructed by summing the details (D) and approximation (A) components. For example, consider a flag $F(t)$ decomposed at a level l (Fig. 3). The detail (D) component detects changes related to high frequency variation in a signal. The approximation (A) component detects gradual changes in the signal, which is the smooth representation of the signal.

The power of DWT lies with the ability to decompose a time series at different levels, and this forms the basis of wavelet MRA. The MRA was used to decompose the NDVI time arrangement from 1982 to 2015 at level 5. Wavelet decomposition at level 5 provides the platform to assess intraannual, interannual variation and human-induced impact on NDVI time series (Martínez and Gilabert 2009; Campos and Marcelo 2012). According to Martínez and Gilabert (2009), in order to select the most appropriate scales for the study of the interannual and intraannual components in vegetation phenology, the scale and frequency need to be connected. The dominant frequency of the wavelet is characterized by defining a purely periodic signal for the period (*p*) (Meyers et al. 1993; Abry 1994) given by:

$$p = \frac{a\Delta t}{V_c} \tag{8}$$

where *a* is the scale; Δt sampling period; and V_c center frequency of the wavelet in Hz (i.e., the frequency corresponding to the spectral peak of the wavelet).

In applying MRA, Daubechies (db) mother wavelet function was utilized because of its ability to identify localized event in time series, its full scaling and translational orthonormality properties and its prevalence in climatic studies (Nalley et al. 2012; Joshi et al. 2016; Liu and Menzel 2016). NDVI decomposition at level 5 is appropriate for recognizing patterns at 30-day, 60-day, 119-day and 238-day scales, and these can be computed using Eq. 8. Thus, D1, D2, D3, D4 and D5 detect trends corresponding to 30 days, 60 days, 119 days, and 238 days, respectively (Table 1) (Martínez and Gilabert 2009; Liu and Menzel 2016). Trends in the details D2 to D5 components and also the approximation (D5) component were analyzed using Mann–Kendall and Sen's Slope to determine an increasing or decreasing magnitude and areas with significant trend at 95% confidence interval. The MRA was executed to decompose NDVI time series per pixels values across the study area.

Mann–Kendall (MK) trend test

Mann–Kendall (MK) is a statistical method for testing trend in time series (Blain 2013). It is nonparametric, which means it does not assume the time series and its deviation from the mean follows any statistical distribution (Dawood and Atta-ur-Rahman 2017). This makes MK powerful for detecting trends in climatic variables which are nonstationary. MK tests for

Table 1 MRA decomposition levels and their corresponding periods (*P*) in days for Daubechies DWT

Level (*j*)	Scale (*a*)	Period (days)	Representation
1	2	60	Rapid changes
2	4	120	Slow rapid changes
3	8	240	Rapid seasonal changes
4	16	360	Slow seasonal changes
5	32	390>	Interannual changes

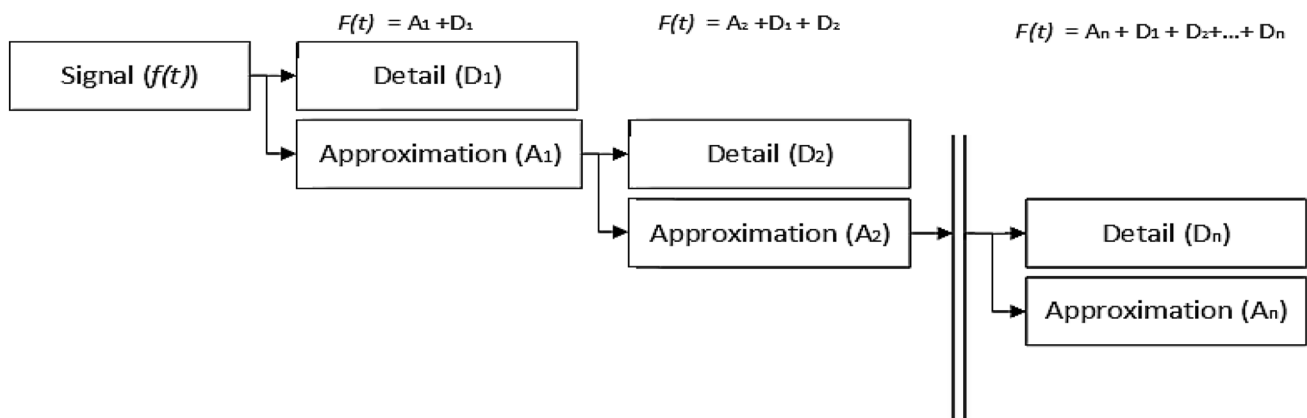$F(t) = A_1 + D_1$ $F(t) = A_2 + D_1 + D_2$ $F(t) = A_n + D_1 + D_2 + ... + D_n$

Fig. 3 Iteration decomposition of DTW into detail (D) and approximation (A) at level *n*

the null hypothesis (H_0) of trend absent against an alternative hypothesis (H_1) of trend which shows upward or downward trend in a time series at a given confidence level. H_0 essentially simply means that the time series is independent and identically distributed around the mean to indicate trend present in a time series (Blain 2013; Nunes and Lopes 2016).

For a given time series (x) with length (N), the test measurement (comparing H_0 and H_1) is given by:

$$\text{Test statistic } (t) = \sum_{i=1}^{N-1} \sum_{j=i+1}^{N} \text{sgn}(x_j - xi) \text{ where } j > 1. \quad (9)$$

If $N > 8$, then the time series is assumed to be normally distributed with a zero mean (Blain 2013) and variance (V) is computed from Eq. (10) as follows:

$$V = \frac{N(N-1)(2N+5) - \sum_{y=1}^{GG} \text{ti}(y-1)(2y+2)y}{18} \quad (10)$$

where GG is the number of groups and ti is the length of GGth group.

The test statistic (t) is standardized and the significance is also estimated by Eq. (11).

$$z = \begin{cases} \frac{t-1}{\sqrt{V}} \rightarrow t > 0 \\ 0 \rightarrow t = 0 \\ \frac{t+1}{\sqrt{V}} \rightarrow t < 0 \end{cases} \quad (11)$$

The null hypothesis is accepted if $|Z| \leq Z_1 - \alpha/2$; otherwise, H_1 is accepted at α significant level.

Sen's slope estimator (Q)

The Sen's Slope estimator (Q) is used to determine the magnitude of trend in a time series. The assertion for Q is that the pattern in the time series is linear (Nunes and Lopes 2016). Negative values of Q suggest a decreasing trend, while positive values imply an increasing trend in a time series. For a given time series (x) of length N, where x_i and x_j are observed or measured values at ith and jth timescale, Q is computed as follows:

$$Q_i = \frac{x_i - x_j}{i - j} \text{ where } i = 1, 2, 3 \ldots N \quad (12)$$

The Q values are computed N times and rearranged in increasing manner. If N is odd, then the median of Q is computed using Eq. (13), but when N is even, the median of Q is computed using Eq. (14):

$$Q_{\text{med}} = Q[N+1]/2 \quad (13)$$

$$Q_{\text{med}} = Q\left[Q_{\frac{N}{2}} + Q_{\frac{N+2}{2}}\right]\Big/2. \quad (14)$$

Results and discussion

The mean NDVI from 1982 to 2015 in UER is shown in Fig. 4. There is high vegetation reflectance in the western and the southern parts of UER, while the northeastern part shows the lowest vegetation.

The results from the wavelet decomposition of spatial aggregated NDVI using Daubechies (db) mother wavelet function from 1982 to 2015 at levelfour (4) are shown in Figs. 5a–f. The NDVI time series was decomposed to level 5. D1 to D5 are the detail (D) components of the original GIMMS NDVI3g time series and represent the short-term fluctuation in the original data. They provide information on vegetation change associated with 60, 120, 240 and 360 days over the 34 years (1982–2015). That is, D1 to D5 were used to assess seasonal and intraannual changes. The approximation (A) component at level 4 of the wavelet decomposition represents long-term trends in the original data (Fig. 5f). Approximation A5 provides information on interannual vegetation changes.

The periodicity in the month to month NDVI time series represents the patterns, and this was analyzed by utilizing CWT to determine the power concentration. Figure 6a is the wavelet power spectrum (WPS) representing the decomposition of NDVI time arrangement into frequency timescale. Figure 6a demonstrates the variance of the power concentration is around the 1-year period, which indicates the variation in NDVI time series in the UER is annually significant. The estimation of the true power in the NDVI time series indicates one significant peak above the 95% confidence interval line, and it is centered around the 1-year period as shown in Fig. 6b. The
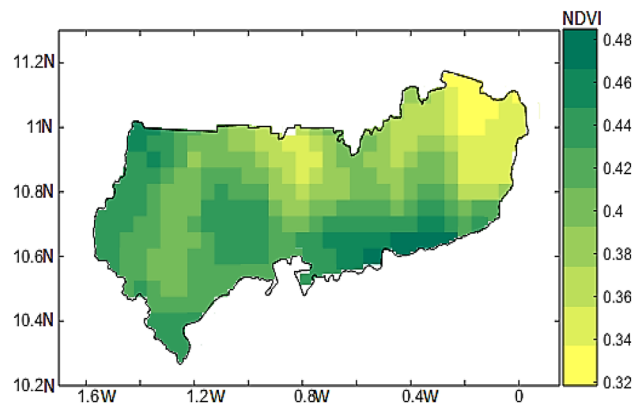

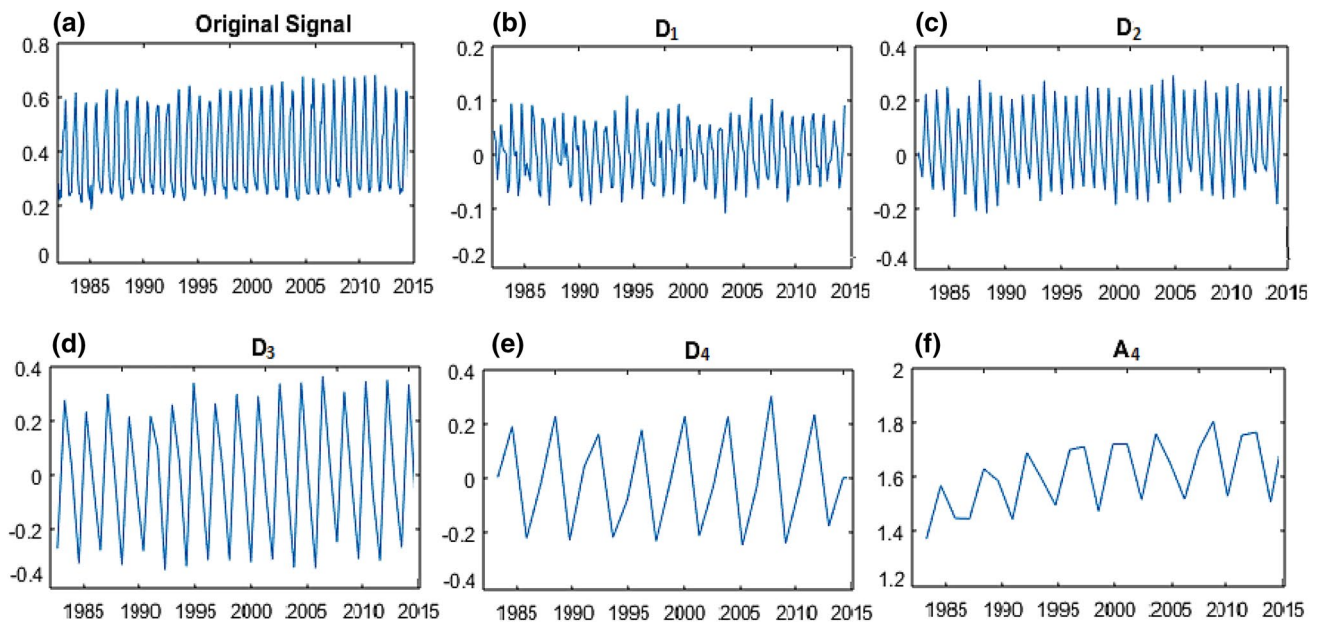**Fig. 4** Mean NDVI from 1982 to 2015

Fig. 5 MRA decomposition of NDVI from 1982 to 2015 at level 4 using Daubechies (db) wavelet function showing the detail (D) and the approximation (A) components
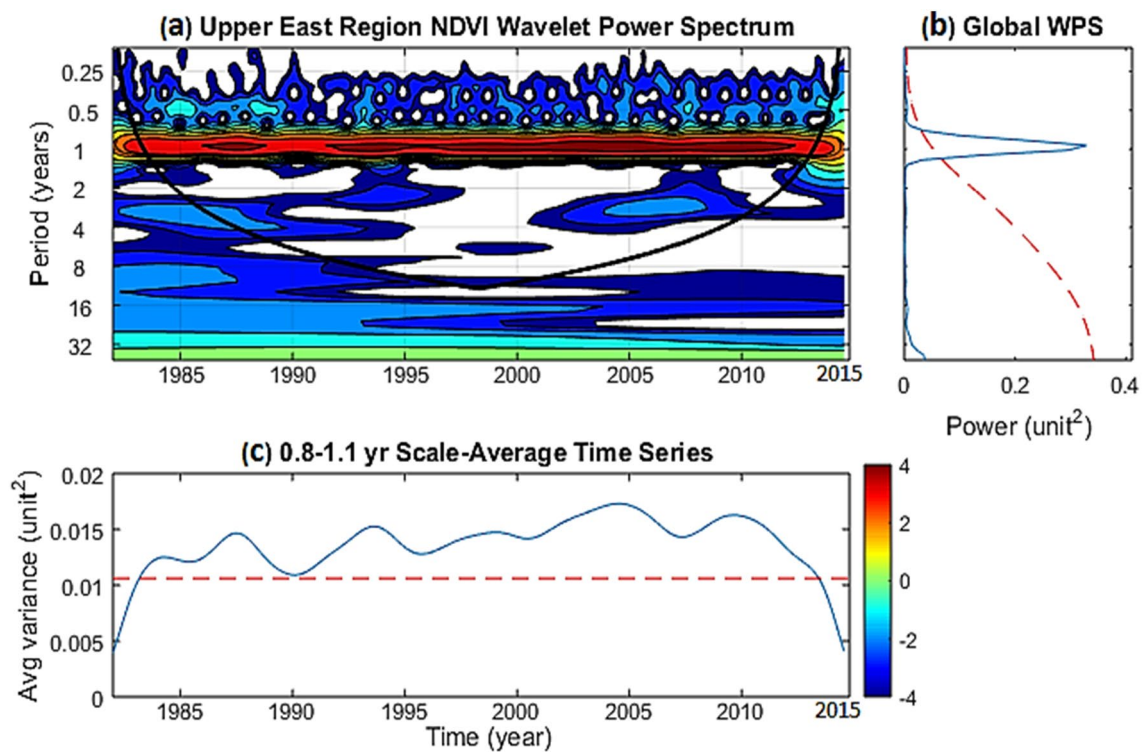

Fig. 6 **a** Wavelet power spectrum which indicates the variance of the power concentration in the time series, **b** global wavelet power spectrum. **c** Scale average of power around 8–11-month period. The red dash lines represent 95% confidence interval

red dash line indicates the 95% confidence interval. Figure 6c is the average variance around 1-year period in the wavelet power spectrum. The varying power concentration shows how NDVI values modulate in the UER. The result indicates a decreasing trend in NDVI from 2010 to 2015.

The intraannual variation of NDVI in the UER was obtained by summing the detail components (D1 to D5). This provides information on how vegetation in UER is changing intraannually (60–360 days). Figure 7a, b shows the Sen's Slope and Mann–Kendall test, respectively, of the intraannual variability in the NDVI time series. The result indicates that UER is experiencing decreasing trend in vegetation performance at the intraannual level. High magnitude of the decreased intraannual vegetation performance is found at the north moving toward the eastern part of UER, which corresponds to areas of low vegetation

(Fig. 4). Figure 7b represents the significant map where the white (H_0) portion indicates areas without significant trend, while the black (H_1) indicates areas of significant trend at 95% confidence interval.

The interannual variability was obtained from the approximation (A5) component. The result from Sen's Slope implies that 4.4% of UER shows decreasing pattern in interannual vegetation performance, while 95.6% shows increasing pattern in the vegetation performance (Fig. 8a–b). Mann–Kendall trend test at 95% confidence interval indicates that 5.2% of the total surface area shows significant pattern (shown in black), while 94.8% showed significant pattern (shown in white). This demonstrates active land degradation (black areas) across the study area and has implication to food security (Fig. 7b) (Antwi-agyei et al. 2012; Yiran et al. 2012).
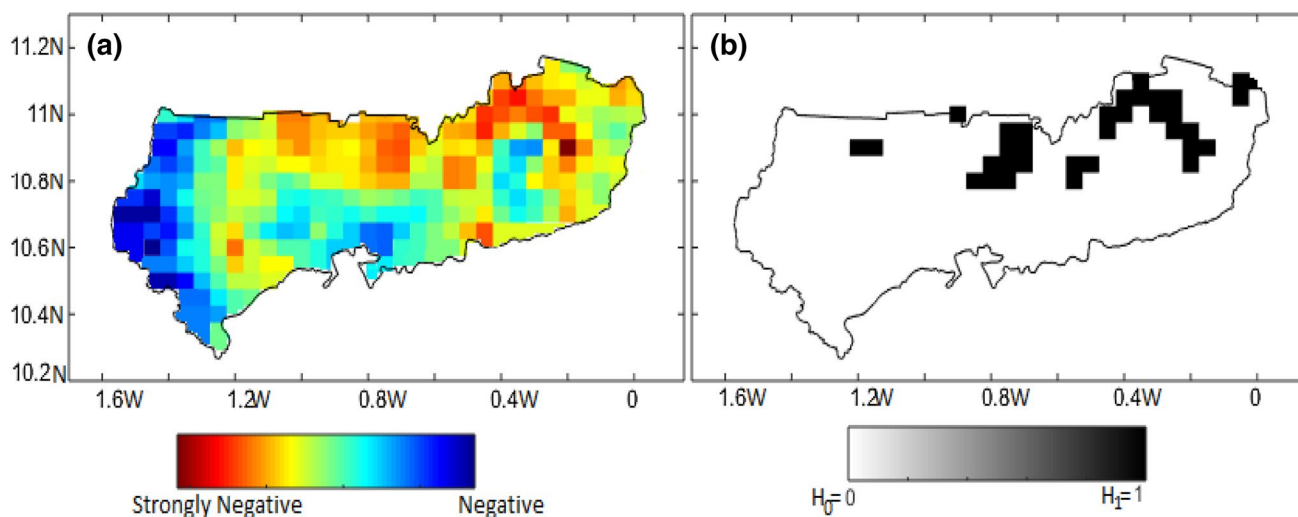

Fig. 7 **a** Sen's Slopes (*Q*) and **b** Mann–Kendall trend test of intraannual NDVI variation from 1982 to 2015
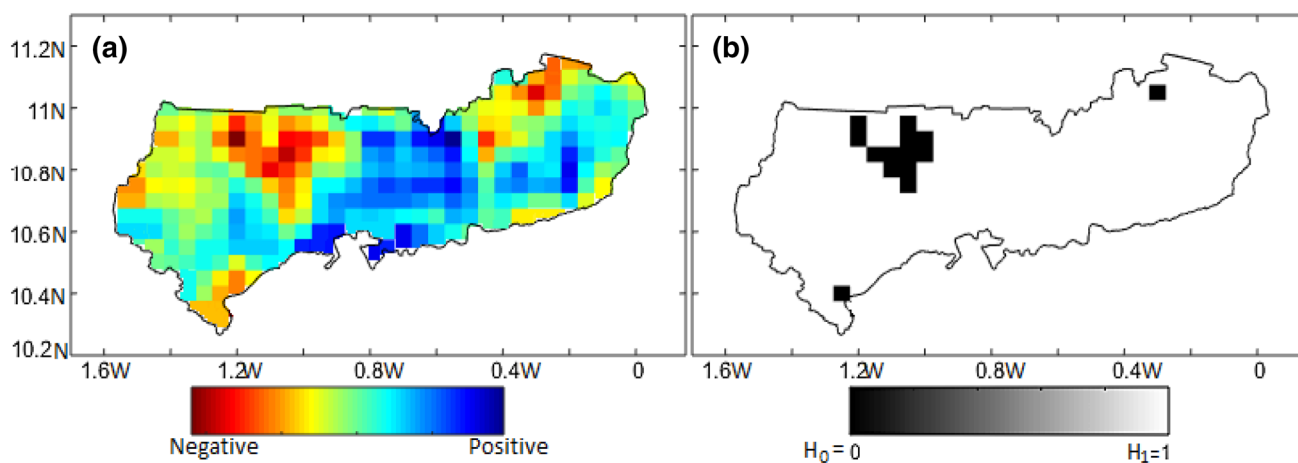

Fig. 8 **a** Sen's Slopes (*Q*) and **b** Mann–Kendall trend test of interannual NDVI variation from 1982 to 2015
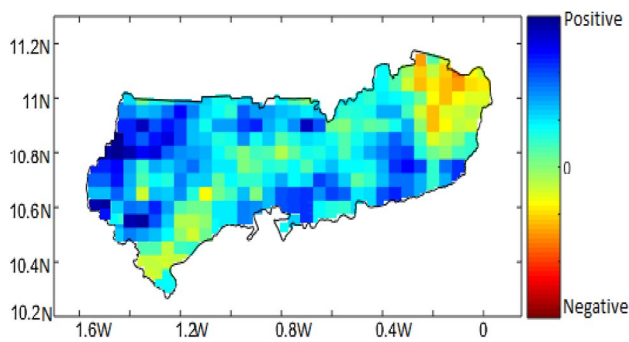
Fig. 9 Trend magnitude at wavelet decomposition five (D5) indicating human-induced factors on NDVI

Further analysis was conducted on the detail component at level 5 (D5). The D5 decomposition represents a major component in describing annual variability. At level 5, all the seasonal factors had been removed and the results show the human-induced factors. The Sen's Slope (Q) result shows that 16.6% of UER indicates a decreasing (negative) trend, while 83.4% shows an increasing (positive) trend (Fig. 9).

The negative trends are concentrated at the northeastern part of UER. The decreasing trend in NDVI can be attributed to the active vegetation degradation as a result of bush burning, deforestation, land erosion, etc. (Yiran et al. 2012). The increasing NDVI can be attributed to fertilizer application by farmers during the farming season and also better land management practices as highlighted by Epule et al. (2012) and Epule et al. (2014) on review on the causes, effects and challenges of Sahelian droughts. The results from the MRA on the NDVI datasets from 1982 to 2015 in the UER indicate that the region has declined in the intraannual vegetation performance. The negative trends in vegetation dynamics at the seasonal, interannual and intraannual scale are mostly concentrated at the northern and northeastern part of UER. This indicates that the decrease in NDVI values at the northeastern part is not only associated with rainfall variation but also vegetation degradation as a result of human activities. The outcome of the research is similar to the findings by USAID (2011), Antwi-agyei et al. (2012) and Yiran et al. (2012). At the interannual scale, 95.6% of the UER shows an increasing trend in NDVI. The increase in NDVI can be attributed to better land management, application of fertilizer and better irrigation farming practices in the UER. Studies by Ichii et al. (2002), Leemhuis et al. (2009), Knauer et al. (2014), Epule et al. (2012) and Epule et al. (2014) indicated significant increase in vegetation dynamics in Africa as the vegetation is recovering from previous drought activities.

Conclusions and recommendations

The MRA was used to detect and quantitatively analyze trends in NDVI time series at the UER from 1982 to 2015. The variation in monthly NDVI in UER is concentrated at 1-year period. The results indicate that there is active vegetation degradation in the UER. At the intraannual scale, almost 100% of the surface area showed decreased magnitude of NDVI time series. The Mann–Kendall significant test at 95% confidence level demonstrates that 11.8% of the surface area shows significant trends. However, 88.2% of the UER shows insignificant trend. At the interannual scale, results indicate that 4.40% of the UER showed significant trend, while 95.60% shows insignificant trend The result from the magnitude of change in NDVI when the 'noise' introduced by seasonality was removed indicates that 16.6% of the surface area showed decreasing trend, while 83.4% showed increasing trend. These results mean that from 1982 to 2015, the vegetation across the UER shows negative performance and 16.6% of the decreased vegetation dynamics are as a result of human activities. The degraded areas are located in the northeastern part moving toward the middle part of UER. For the long-term analysis, the vegetation showed a significant increase across the UER with some selected parts indicating decreased vegetation as a result of climatic variables. From the investigation, the drivers of vegetation degradation in the UER are human activities and climate change. The outcome from this study provides a benchmark for effective and efficient management, planning and sustainable development since the UER is located in the transition zone between Sahelian savanna and Guinean savanna.

Compliance with ethical standards

Conflict of interest The authors declare that they have no conflict of interest.

References

Abry P (1994) Transformées en ondelettes: analyses multirésolution et signaux de pression en turbulence (Doctoral dissertation, Lyon 1)

Al-Bakri J, Taylor J (2003) Application of NOAA AVHRR for monitoring vegetation conditions and biomass in Jordan. J Arid Environ 54:579–593. https://doi.org/10.1006/jare.2002.1081

Antwi-agyei P, Fraser EDG, Dougill AJ, Stringer LC, Simelton E (2012) Mapping the vulnerability of crop production to drought in Ghana using rainfall, yield and socioeconomic data. Appl Geogr 32(2):324–334. https://doi.org/10.1016/j.apgeog.2011.06.010

Awotwi A, Yeboah F, Kumi M (2015) Assessing the impact of land cover changes on water balance components of White Volta

Basin in West Africa. Water Environ J 29(2):259–267. https://doi.org/10.1111/wej.12100

Awotwi A, Anornu GK, Quaye-Ballard JA, Annor T, Forkuo EK, Harris E, Agyekum J, Terlabie JL (2019) Water balance responses to land-use/land-cover changes in the Pra River Basin of Ghana, 1986–2025. CATENA 182:104129. https://doi.org/10.1016/j.catena.2019.104129

Ayumah R (2016) Climate variability and food crop production in the Bawku. MPhil. Thesis, Department of Geography and Rural Development, Kwame Nkrumah University of Science and Technology, Kumasi, Ghana

Baidu M, Amekudzi LK, Aryee JNA, Annor T (2017) Assessment of long-term spatio-temporal rainfall variability over Ghana using wavelet analysis. Climate 5(30):1–24. https://doi.org/10.3390/cli5020030

Blain GC (2013) The modified Mann–Kendall test: on the performance of three variance correction approaches. Bragantia 72(4):416–425. https://doi.org/10.1590/brag.2013.045

Bruce LM, Byrd JD (2006) Denoising and wavelet-based feature extraction of MODIS multi-temporal vegetation signatures. GIScience Remote Sens 43(1):170–180. https://doi.org/10.2747/1548-1603.43.1.67

Campos AN, Di Bella CM (2012) Multi-temporal analysis of remotely sensed information using wavelets. J Geogr Inf Syst 4:383–391. https://doi.org/10.4236/jgis.2012.44044

Dahlin K, Fisher R, Lawrence P (2015) Environmental drivers of drought deciduous phenology. Biogeosciences 12:5061–5074. https://doi.org/10.5194/bg-12-5061-2015

Dawood M (2017) Spatio-statistical analysis of temperature fluctuation using Mann–Kendall and Sen' s slope approach. Clim Dyn 48(3):783–797. https://doi.org/10.1007/s00382-016-3110-y

Dyn C, Zhang J, Hao Y, Hu BX, Huo X, Hao P (2016) The effects of monsoons and climate teleconnections on the Niangziguan Karst Spring discharge in North China. Clim Dyn 48(1):53–70. https://doi.org/10.1007/s00382-016-3062-2

Epinat V, Stein A, de Jong SM, Bouma J (2001) A wavelet characterization of high-resolution NDVI patterns for precision agriculture. Int J Appl Earth Obs Geoinf 3(2):121–132. https://doi.org/10.1016/S0303-2434(01)85003-0

Epule ET, Peng C, Lepage L, Nguh BS, Mafany NM (2012) Can the African food supply model learn from the Asian food supply model? Quantification with statistical methods. Environ Dev Sustain 14(4):593–610. https://doi.org/10.1007/s10668-012-9341-0

Epule ET, Peng C, Lepage L, Chen Z (2014) The causes, effects and challenges of Sahelian droughts: a critical review. Reg Environ Change 14(1):145–156. https://doi.org/10.1007/s10113-013-0473-z

Galford GL, Mustard JF, Melillo J, Gendrin A, Cerri CC, Cerri CEP (2008) Wavelet analysis of MODIS time series to detect expansion and intensification of row-crop agriculture in Brazil. Remote Sens Environ 112:576–587. https://doi.org/10.1016/j.rse.2007.05.017

GeerkenR Ilaiwi M (2004) Assessment of rangeland degradation and development of a strategy for rehabilitation. Remote Sens Environ 90(4):490–504. https://doi.org/10.1016/j.rse.2004.01.015

Ghana Statistical Service (2014) 2010 Population and Housing Census: District Analytical Report. Nabdom District. Retrieved from http://www2.statsghana.gov.gh/docfiles/2010_District_Report/Upper%20East/NABDAM.pdf

Ibrahim YZ, Balzter H, Kaduk J, Tucker CJ (2015) Land degradation assessment using residual trend analysis of GIMMS NDVI3g, soil moisture and rainfall in Sub-Saharan West Africa from 1982 to 2012. Remote Sens 7:5471–5494. https://doi.org/10.3390/rs70505471

Ichii K, Kawabata A, Yamaguchi Y (2002) Global correlation analysis for NDVI and climatic variables and NDVI trends: 1982–1990. Int

J Remote Sens 23(18):3873–3878. https://doi.org/10.1080/01431160110119416

Jia K, Liang S, Wei X, Yao Y, Su Y, Jiang B, Wang X (2014) Land cover classification of Landsat data with phenological features extracted from time series MODIS NDVI data. Remote Sens 6:11518–11532. https://doi.org/10.3390/rs61111518

Joshi N, Gupta D, Suryavanshi S, Adamowski J, Madramootoo CA (2016) Analysis of trends and dominant periodicities in drought variables in India: a wavelet transform based approach. Atmos Res 182:200–220. https://doi.org/10.1016/j.atmosres.2016.07.030

Knauer K, Gessner U, Dech S, Kuenzer C (2014) Remote sensing of vegetation dynamics in West Africa. Int J Remote Sens 35(17):6357–6396. https://doi.org/10.1080/01431161.2014.954062

Leemhuis C, Jung G, Kasei R, Liebe J (2009) The Volta Basin water allocation system: assessing the impact of small-scale reservoir development on the water resources of the Volta basin, West Africa. Adv Geosci 21:57–62

Liu Z, Menzel L (2016) Identifying long-term variations in vegetation and climatic variables and their scale-dependent relationships: a case study in Southwest Germany. Glob Planet Change 147:54–66. https://doi.org/10.1016/j.gloplacha.2016.10.019

Lunetta RS, Knight JF, Ediriwickrema J, Lyon JG, Worthy LD (2006) Land-cover change detection using multi-temporal MODIS NDVI data. Remote Sens Environ 105(2):142–154. https://doi.org/10.1016/j.rse.2006.06.018

Martínez B, Gilabert MA (2009) Vegetation dynamics from NDVI time series analysis using the wavelet transform. Remote Sens Environ 113(9):1823–1842. https://doi.org/10.1016/j.rse.2009.04.016

Mberego S, Sanga-ngoie K, Kobayashi S (2013) Vegetation dynamics of Zimbabwe investigated using NOAA-AVHRR NDVI from 1982 to 2006: a principal component analysis. Int J Remote Sens 34(19):6764–6779. https://doi.org/10.1080/01431161.2013.80683

Meyers SD, Kelly BG, Brien JJ (1993) An introduction to wavelet analysis in oceanography and meteorology: with application to the dispersion of Yanai waves. Mon Weather Rev 121(10):2858–2866. https://doi.org/10.1175/1520-0493(1993)121%3c2858:AITWAI%3e2.0.CO;2

Ministry of Food and Agriculture, Ghana (2017) Upper East Region. Retrieved from http://mofa.gov.gh/site/?page_id=654

Nalley D, Adamowski J, Khalil B (2012) Using discrete wavelet transforms to analyze trends in streamflow and precipitation in Quebec and Ontario (1954–2008). J Hydrol 475:204–228. https://doi.org/10.1016/j.jhydrol.2012.09.049

Nischitha V, Ahmed SA, Varikoden H, Revadekar JV, Ahmed SA, Varikoden H, Revadekar JV (2014) The impact of seasonal rainfall variability on NDVI in the Tunga and Bhadra river basins, Karnataka, India. Int J Remote Sens 35(23):8025–8043. https://doi.org/10.1080/01431161.2014.979301

Nunes AN, Lopes P (2016) Streamflow response to climate variability and land-cover changes in the River Beça Watershed, Northern Portugal. River Basin Manag. https://doi.org/10.5772/63079

Omuto CT, Vargas RR, Alim MS, Paron P (2010) Mixed-effects modelling of time series NDVI-rainfall relationship for detecting human-induced loss of vegetation cover in drylands. J Arid Environ 74(11):1552–1563. https://doi.org/10.1016/j.jaridenv.2010.04.001

Ramana RV, Krishna B, Kumar SR (2013) Monthly rainfall prediction using wavelet neural network analysis. Water Resour Manag 27:3697–3711. https://doi.org/10.1007/s11269-013-0374-4

Rimkus E, Stonevicius E, Kilpys J, Mac V, Valiukas D (2017) Drought identification in the Eastern Baltic region using NDVI. Earth Syst Dyn 5:1–15. https://doi.org/10.5194/esd-2017-5

Röder A, Hill J (eds) (2009) Recent advances in remote sensing and geoinformation processing for land degradation assessment. CRC Press, Boca Raton

Santos CAG, Freire PKMM (2012) Analysis of precipitation time series of Urban Centers of Northeastern Brazil using wavelet transform. Int J Environ Chem Ecol Geol Geophys Eng 6(7):405–410

Sharma A (2006) Spatial data mining for drought monitoring: an approach using temporal NDVI and rainfall relationship. MSc. Thesis, International Institute for Geo-information Science and Earth Observation

Sprugel DG (1991) Disturbance, equilibrium and environmental variability: what is "Natural" vegetation in a changing environment? Biol Conserv 58(1):1–18. https://doi.org/10.1016/0006-3207(91)90041

Stanturf JA, Warren ML Jr, Charnley S, Polasky SC, Goodrick SL, Armah F, Nyako YA (2011) Ghana climate change vulnerability and adaptation assessment. USAID, Washington, DC

Sun T, Ferreira VG, He X, Andam-akorful SA (2016) Water availability of São Francisco River Basin based on a space-borne geodetic sensor. Water. https://doi.org/10.3390/w8050213

Torrence C, Compo GP (1998) A practical guide to wavelet analysis. Bull Am Meteorol Soc 79(1):61–78. https://doi.org/10.1175/1520-0477(1998)079%3c0061:APGTWA%3e2.0.CO;2

Yiran GAB, Kusimi JM, Kufogbe SK (2012) A synthesis of remote sensing and local knowledge approaches in land degradation assessment in the Bawku East District, Ghana. Int J Appl Earth Obs Geoinf 14(1):204–213. https://doi.org/10.1016/j.jag.2011.09.016

Publisher's Note Springer Nature remains neutral with regard to jurisdictional claims in published maps and institutional affiliations.